

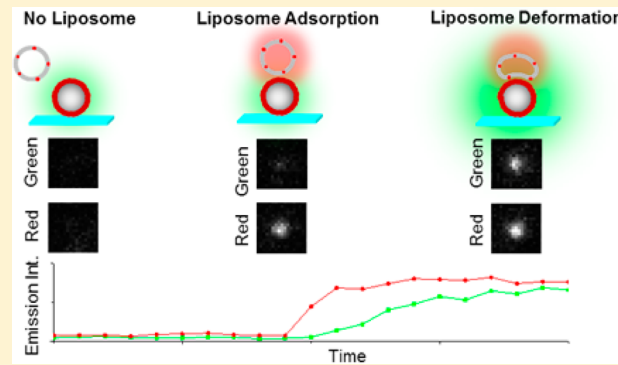
Exploiting Conjugated Polyelectrolyte Photophysics toward Monitoring Real-Time Lipid Membrane-Surface Interaction Dynamics at the Single-Particle Level

Christina F. Calver, Hsiao-Wei Liu, and Gonzalo Cosa*

Department of Chemistry and Centre for Self Assembled Chemical Structures (CSACS/CRMAA), McGill University, 801 Sherbrooke Street West, Montreal, QC H3A 0B8, Canada

Supporting Information

ABSTRACT: Herein we report the real-time observation of the interaction dynamics between cationic liposomes flowing in solution and a surface-immobilized charged scaffolding formed by the deposition of conjugated polyanion poly[5-methoxy-2-(3-sulfopropoxy)-1,4-phenylenevinylene] (MPS-PPV) onto 100-nm-diameter SiO₂ nanoparticles (NPs). Contact of the freely floating liposomes with the polymer-coated surfaces led to the formation of supported lipid bilayers (SLBs). The interaction of the incoming liposomes with MPS-PPV adsorbed on individual SiO₂ nanoparticles promoted the deaggregation of the polymer conformation and led to large emission intensity enhancements. Single-particle total internal reflection fluorescence microscopy studies exploited this phenomenon as a way to monitor the deformation dynamics of liposomes on surface-immobilized NPs. The MPS-PPV emission enhancement (up to 25-fold) reflected on the extent of membrane contact with the surface of the NP and was correlated with the size of the incoming liposome. The time required for the MPS-PPV emission to reach a maximum (ranging from 400 to 1000 ms) revealed the dynamics of membrane deformation and was also correlated with the liposome size. Cryo-TEM experiments complemented these results by yielding a structural view of the process. Immediately following the mixing of liposomes and NPs the majority of NPs had one or more adsorbed liposomes, yet the presence of a fully formed SLB was rare. Prolonged incubation of liposomes and NPs showed completely formed SLBs on all of the NPs, confirming that the liposomes eventually ruptured to form SLBs. We foresee that the single-particle studies we report herein may be readily extended to study membrane dynamics of other lipids including cellular membranes in live cell studies and to monitor the formation of polymer-cushioned SLBs.



INTRODUCTION

In cells, the ability of lipid membranes to dynamically adjust phase and topology is essential for processes such as vesicle trafficking, cell division, and the formation of complex organelle structures.^{1,2} These structural changes require the generation of highly strained membranes whose unfavorable curvature is stabilized by the interplay of electrostatic and hydrophobic interactions with charged biopolymers such as proteins.^{1–5} The combination of lipid composition and biopolymer scaffolding results in a rich array of possible forms and textures; this structural diversity has profound implications not only for cell biology but also for biotechnological applications (e.g., gene delivery via lipoplexes^{6,7} or the formation of supported lipid bilayers).^{8,9} In this regard, although techniques such as cryo-electron microscopy are able to resolve the structural changes that result from lipid–polymer interactions on the nanoscale,^{10–13} the dynamics of how these rearrangements occur are difficult to determine experimentally.

Here, we report an approach to determine the dynamics of lipid–polymer interactions at the single-particle level by monitoring the fluorescence enhancement of a conjugated

polyelectrolyte adsorbed on a solid scaffold upon encountering single liposomes. The photophysical properties of conjugated polymers and their charged counterparts, conjugated polyelectrolytes, have been shown to be intimately related to chain conformation.^{14–18} Collapsed polymer conformations favor efficient energy transfer to nonemissive trap sites, resulting in a low fluorescence quantum yield.^{15,17,19} Deaggregation of the polymer backbone through interaction with surfactants,^{20–23} including lipids,^{24–29} reduces the efficiency of energy transfer and leads to highly increased fluorescence quantum yields. We reasoned that morphological changes experienced by conjugated polyelectrolytes upon contact with a lipid bilayer would lead to spectroscopic changes that could be monitored in real time to unmask the dynamics of membrane deformation on a curved, polymer-coated surface.

Conjugated polyanion poly[5-methoxy-2-(3-sulfopropoxy)-1,4-phenylenevinylene] (MPS-PPV) was adsorbed onto the

Received: March 17, 2015

Revised: April 28, 2015

Published: May 8, 2015



surface of amino-functionalized 100-nm-diameter silica nanoparticles (NPs), and the NPs were in turn immobilized onto a coverslip for single-molecule imaging.^{30,31} Using total internal reflection fluorescence microscopy (TIRFM) with a two-color detection scheme, we were able to monitor in real time the encounter and subsequent deformation of incoming liposomes prepared from cationic lipid 1,2-dioleoyl-3-trimethylammonium-propane (DOTAP) on the surface of the NPs. Deaggregation of MPS-PPV upon interaction with excess liposomes led to dramatic (average 23-fold) MPS-PPV emission intensity enhancements. When liposomes were flowed at a lower concentration such that the interaction of individual liposomes could be observed one at a time, the magnitude of the enhancements was related to the liposome size, reflecting on the percentage of NP surface area in contact with the adsorbed liposome and thus providing a measure of liposome deformability. Cryo-TEM micrographs obtained from samples vitrified immediately after mixing further showed adsorbed liposomes deforming to accommodate the curvature of the NPs. Prolonged incubation of liposomes and NPs showed in turn completely formed supported lipid bilayers (SLBs) on all of the NPs after 30 min, confirming that the liposomes eventually ruptured. The liposome size and the enhancement period (ranging from 400 to 1000 ms) were found to be correlated, providing insight into the time required for the liposome to deform on the surface of the NP and for MPS-PPV to deaggregate within the membrane.

Given the plethora of conjugated polyelectrolytes currently available^{32,33} where the backbone and charge may be independently tailored toward enhancing electrostatic and/or hydrophobic interactions with lipids,^{25,34,35} we foresee that the strategy we report herein toward measuring model lipid membrane dynamics in the presence of a charged scaffolding may be readily extended to a diverse range of lipids and lipid mixtures, including cellular membranes, and may be further exploited with respect to the study of the formation of polymer-cushioned SLBs.

EXPERIMENTAL SECTION

Aminosilanization of SiO₂ NPs. The surface charge of the SiO₂ NPs was rendered positive by reaction with an aminosilane to facilitate the deposition of MPS-PPV by electrostatic attraction between the negatively charged sulfonate groups of the polyanion and the positively charged amine groups of the functionalized SiO₂ NPs. A 400 μL aliquot of 5.32% (w/w) SiO₂ NPs in water (Polysciences, Inc.) was transferred to a 1.5 mL Eppendorf tube. (3-Aminopropyl)-trimethoxsilane (Sigma-Aldrich) (2.0 μL, 12 μmol) was added with vigorous vortex mixing. The reaction mixture was incubated at room temperature (22–25 °C) for 5 min. Hydrochloric acid (8 μL, 3 M) was added next to protonate the amine groups and quench any unreacted aminosilane. The mixture was immediately centrifuged at 16 060 g for 5 min. Approximately 90% of the supernatant was removed and replaced with an equal volume of water. The NPs were then resuspended by sonication/vortex mixing. The washing cycle was repeated until the pH of the supernatant was ca. 4. The final concentration of the SiO₂NH₃⁺ NPs was 65 nM in terms of the number of NPs.

MPS-PPV Adsorption on SiO₂NH₃⁺ NPs. To adsorb MPS-PPV onto the surface of the SiO₂NH₃⁺ NPs, a suspension of NPs was added to excess MPS-PPV. The presence of excess MPS-PPV prevented the aggregation of NPs by polymer bridging. SiO₂NH₃⁺ (20 μL, 65 nM) was added to 0.230 mL of water and 0.250 mL of methanol in a 1.5 mL Eppendorf tube. This SiO₂NH₃⁺ suspension was added, 10 μL at a time, to 1.00 mL of 3 mM MPS-PPV (concentration in terms of polymer repeat units) in 1:1 water/methanol with vigorous vortex

mixing. The mixture was agitated gently at room temperature for ca. 30 min and then centrifuged at 16 060g for 5 min. The supernatant containing unadsorbed MPS-PPV was removed and replaced with an equal volume of water, and the NPs were resuspended by sonication/vortex mixing. This washing cycle was repeated until traces of MPS-PPV could no longer be detected in the absorbance spectrum of the supernatant. The final concentration of MPS-PPV-coated NPs was 1.3 nM in terms of the number of NPs. The MPS-PPV-coated NPs were stored at 4 °C and protected from light.

Preparation of DOTAP Liposomes. To prepare liposomes, 1,2-dioleoyl-3-trimethylammonium-propane chloride salt (DOTAP) powder (Avanti Lipids Corp.) was dissolved in chloroform to a concentration of 0.10 mg/mL. Fifty microliters of this solution was transferred to a small glass vial. The vial was rotated under a stream of argon to evaporate the solvent, forming a thin lipid film along the walls of the vial. The vial was placed under vacuum for an additional 30 min to remove traces of solvent. The dried film was rehydrated in 358 μL of 3 mM NaCl aqueous solution to a final lipid concentration of 20 mM. The suspension was vortex mixed briefly to loosen the film adhering to the walls of the vial. For 100 nm liposomes, the suspension was taken through eight freeze/thaw cycles (5 min on dry ice followed by 5 min in a sonicator bath) to increase the unilamellarity of the liposomes. The suspension was then extruded 11 times through a 100 nm polycarbonate membrane using a miniextruder (Avanti Lipids Corp.). For 400 nm liposomes, the procedure was identical except that the suspension was not subjected to any freeze/thaw cycles and a 400 nm polycarbonate membrane was used instead of a 100 nm membrane. For liposomes containing lipophilic dye 1,1'-dioctadecyl-3,3,3',3'-tetramethylindodicarbocyanine perchlorate (DiD), the procedure was identical except that an aliquot of DiD dissolved in ethanol was added to the lipids dissolved in chloroform prior to forming the lipid film. The liposomes were stored at 4 °C and protected from light.

Absorption and Fluorescence Measurements. Absorption and emission spectra were recorded on a Hitachi U2800 spectrophotometer and a Photon Technology International Inc. fluorimeter, respectively. The MPS-PPV-coated NPs were diluted to a concentration of ~0.1 nM in water before acquiring the spectra. The amount of MPS-PPV adsorbed on the NPs was estimated by subtracting the absorbance due to scattering from a blank consisting of uncoated NPs from the absorbance of the NPs with adsorbed MPS-PPV. The sample was excited at 450 nm and the emission spectrum was recorded between 470 and 800 nm, unless otherwise noted.

Formation of DOTAP Supported Lipid Bilayers on MPS-PPV-Coated SiO₂ NPs. The formation of DOTAP-supported lipid bilayers on the MPS-PPV-coated SiO₂ NPs was accomplished by incubating a suspension of NPs with excess DOTAP liposomes. In our protocol, 1.5 mL of 0.11 nM MPS-PPV-coated SiO₂ NPs in water was added 10 μL at a time to 1.5 mL of 1 mM (in terms of lipid) DOTAP liposomes (13 nM in 100-nm-diameter liposomes) in Hyclone molecular biology grade water (ThermoScientific) containing 3 mM NaCl with vigorous vortex mixing. The mixture was centrifuged for 5 min at 16 060g, and the supernatant containing excess liposomes was removed and replaced with an equal volume of water. The bright-orange pellet was resuspended by sonication and vortex mixing. The final concentration of MPS-PPV-coated NPs with DOTAP was 0.055 nM. For imaging by cryo-TEM, 10× concentrated samples were used. Specifically, 80 nM DOTAP liposomes 400 nm in diameter and 1.1 nM MPS-PPV-coated NPs were mixed and vitrified within 30 s of mixing.

Monitoring the Rupture of DOTAP Liposomes in Contact with MPS-PPV-Coated SiO₂ NPs. DOTAP films were rehydrated in a 3 mM NaCl aqueous solution containing 317 μM sulfo-Cy5 carboxylic acid (Lumiprobe) to a final lipid concentration of 20 mM. At this lipid concentration, the volume fraction of the liposomes in solution is 0.07, leading to a theoretical encapsulation efficiency of Cy5 molecules of 7%. The liposomes were then subjected to eight freeze/thaw cycles and extruded though a 100 nm polycarbonate membrane. The liposomes were separated from unencapsulated Cy5 using size exclusion chromatography. DOTAP liposomes (sacrificial liposomes containing no Cy5) (200 μL, 20 mM) were run through a size

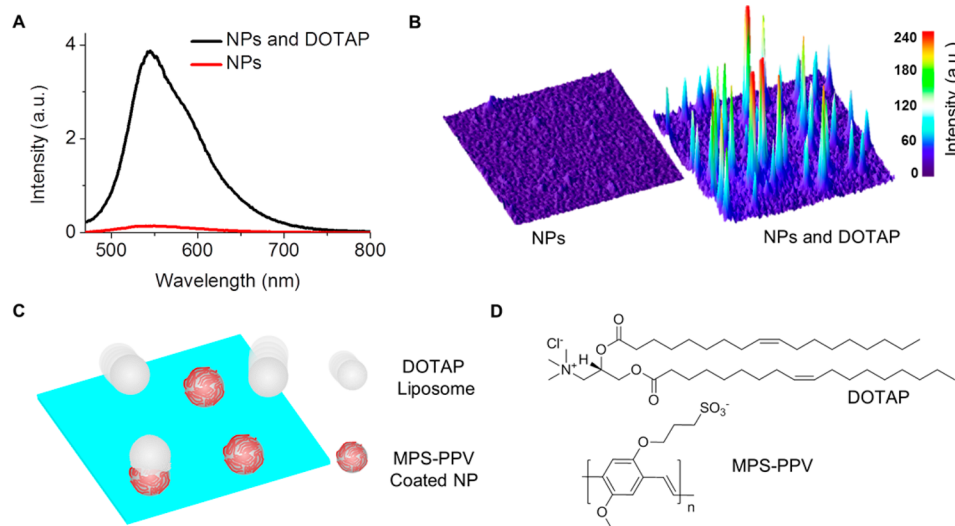


Figure 1. Ensemble and single-nanoparticle studies of the emission enhancement of MPS-PPV adsorbed on SiO_2 NPs triggered by interaction with DOTAP liposomes. (A) Emission spectra of 0.1 nM MPS-PPV-coated NPs before (red circles) and after (black squares) addition to 13 nM 100 nm DOTAP liposomes in 3 mM NaCl. (B) Surface plot of MPS-PPV emission intensity obtained by TIRFM before and after 100-nm-diameter DOTAP liposomes 13 nM in concentration were flowed over surface-bound MPS-PPV-coated NPs. (C) Cartoon illustrating the interaction mechanisms between MPS-PPV-coated NPs adsorbed on the surface of a glass coverslip and DOTAP liposomes flowed over the surface. (D) Chemical structures of DOTAP and MPS-PPV.

exclusion column packed with Sephadryl S500HR (Sigma-Aldrich) to prime the column. Next, 200 μL of 20 mM DOTAP containing Cy5 was loaded onto the column. Liposomes containing encapsulated Cy5 molecules eluted in earlier fractions whereas unencapsulated (free) Cy5 had a longer retention time. 0.011 nM DOTAP containing encapsulated Cy5 was added to 0.11 nM MPS-PPV-coated NPs in either 300 μM FeCl_3 or a control containing no FeCl_3 . The Cy5 emission spectrum was monitored immediately and 10 min after mixing. The amount of Cy5 quenching by FeCl_3 was proportional to the number of liposomes that formed rupture pores within the 10 min time period. The effectiveness of this method was confirmed by a control experiment where identical samples were subjected to 5 min of freezing on dry ice followed by 5 min of thawing in a water bath. The freeze/thaw cycle mechanically disrupted the lipid membrane, exposing the encapsulated Cy5 molecules to FeCl_3 , resulting in a nearly complete quenching of their emission.

TIRFM Imaging. Glass coverslips were cleaned and functionalized with amine groups in preparation for imaging the MPS-PPV-coated SiO_2 NPs using TIRFM microscopy. Glass jars containing eight coverslips were filled with piranha solution [1 part 30% hydrogen peroxide (Fisher Scientific) and 2 parts concentrated sulfuric acid (ACP Chemicals)] and left to soak for ca. 1 h. The coverslips were then rinsed three times with Hyclone molecular biology grade water (ThermoScientific) and three times with acetone (HPLC grade, Fisher). The coverslips were immersed in 25 mL of acetone and 0.50 mL of Vectabond (Vector Laboratories). The mixture was agitated gently and incubated for 5 min. The acetone/Vectabond mixture was poured out, and the reaction was quenched by rinsing with 2 \times 25 mL of water. The coverslips were dried under a stream of nitrogen prior to being fitted with flow chambers. The flow chambers were prepared with a predrilled polycarbonate film (Grace Biolabs) and assembled on top of the coverslips. Silicone ports were glued on top of the chamber with double-sided tape. The volume of the sample chamber was ca. 10 μL .

Electrostatic interactions with the positively charged glass coverslip allowed for the selective adsorption of the negatively charged MPS-PPV-coated SiO_2 NPs on the surface while preventing the nonspecific adsorption of the positively charged DOTAP liposomes. A good surface density of NPs was achieved by injecting 20 μL of 50 pM MPS-PPV-coated NPs in water into the sample chamber and incubating for ca. 1 min. A total of 5 \times 20 μL of 3 mM NaCl was then injected to wash away any NPs that were not bound to the surface. Images were

acquired while flowing liposome suspensions in 3 mM NaCl aqueous solutions at a rate of 5 $\mu\text{L}/\text{min}$ through the chamber using a syringe pump (Harvard Apparatus PHD 2000 Infusion). All experiments were conducted at room temperature (22–25 °C).

The imaging experiments were performed using an Olympus IX71 microscope adapted with an Olympus IX2-RFAEVA-2 turnkey TIRFM module. The excitation source was either the 488 or 514 nm output of a continuous wave argon ion laser (SpectraPhysics). The laser power measured out of the objective was 220 μW for the 488 nm excitation and 580 μW for the 514 nm excitation (ca. 1.0 and 2.6 W cm^{-2} , respectively). The laser beam was introduced by a single-mode fiber optic and was directed by a dichroic beamsplitter (z488rdc or z514rdc, Chroma) to the sample via a high numerical aperture (N.A. = 1.45) oil-immersion objective (Olympus PLAN APO 60 \times). The fluorescence emission was collected through the same objective and was then transmitted through an emission filter (HQ500 LP or HQ530 LP, Chroma) and was then separated into two emission channels by a series of dichroic mirrors (640dcxr, Chroma). The images were acquired at an acquisition rate of 50–100 ms using a Cascade 512B EMCCD camera (Roper Scientific, Inc.) controlled by Image Pro software. Intensity versus time trajectories were extracted from background-subtracted images processed using a home-built Matlab routine based on algorithms previously reported by the Ha group.³⁶

Cryogenic Transmission Electron Microscopy. To prepare the samples for imaging, 5 μL of sample was added to glow-discharged QUANTIFOIL R 2/2 copper grids. Samples were blotted and frozen hydrated by plunging into a bath of liquid ethane slush. The samples were stored at liquid-nitrogen temperature until transfer to a 626 Single Tilt Cryotransfer System (Gatan Inc.) and observed with an FEI G2 F20 cryo-STEM microscope operated at 200 kV (FEI, Inc.). Images were recorded on a Gatan Ultrascan 4k \times 4k Digital (CCD) Camera System camera at a nominal magnification of 50 000 \times at a defocus level of 4 μm . Samples consisted of MPS-PPV-coated NPs, MPS-PPV-coated NPs incubated for 30 min with 80 nM DOTAP liposomes (excess liposomes were removed by centrifugation), and MPS-PPV-coated NPs mixed with 80 nM DOTAP liposomes immediately before vitrifying. The MPS-PPV-coated NP concentration was 1.1 nM for all samples.

Dynamic Light Scattering Measurements. DLS measurements were acquired using a Malvern Zetasizer Nano ZS equipped with a 633 nm red laser. The samples were equilibrated to a temperature of 25 °C

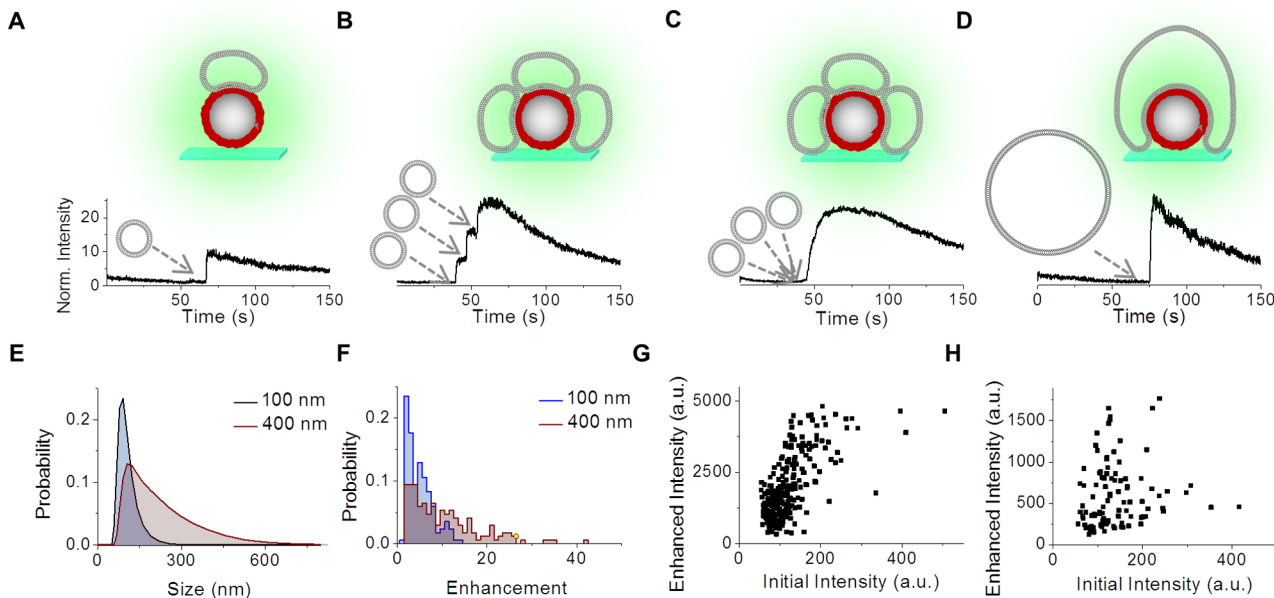


Figure 2. Enhancement intensities and dynamics for individual MPS-PPV-coated NPs in response to 100 and 400 nm DOTAP liposomes. Surface-immobilized MPS-PPV-coated NPs were excited with a 488 nm laser ($220 \mu\text{W}$), and TIRFM images were obtained at a time resolution of 10 frames/s while flowing liposome solutions at a rate of $5 \mu\text{L}$ per min. (A–D) Representative fluorescence intensity versus time trajectories obtained under the following conditions: (A) 0.13 nM 100 nm liposomes; (B) 1.3 nM 100 nm liposomes; (C) 13 nM 100 nm liposomes; and (D) 0.08 nM 400 nm liposomes. The trajectories were normalized by the intensity of the NP immediately before the enhancement. (E) Size distribution of 100 and 400 nm DOTAP liposomes obtained by dynamic light scattering. (F) Histogram of enhancements recorded while flowing solutions of 0.13 nM 100 nm liposomes and 0.08 nM 400 nm liposomes. Enhancements were determined for 170 MPS-PPV-coated NPs under both conditions. (G, H) Correlation plots between the initial intensity of MPS-PPV-coated NPs and their enhanced intensity after flowing 400 nm liposomes at a high concentration of 8 nM and at a low concentration of 0.08 nM, respectively.

and diluted to a concentration of approximately 0.1 nM in terms of the number of particles.

RESULTS AND DISCUSSION

Ensemble Studies on the Interaction of DOTAP Liposomes with MPS-PPV. We first explored at the ensemble level the interaction of MPS-PPV-coated NPs with 100-nm-diameter DOTAP liposomes by adding a suspension of NPs to a 100-fold excess of 100-nm-diameter liposomes (final concentrations of 0.1 and 13 nM, respectively). To prepare the MPS-PPV-coated NPs, we adapted a previously reported method to functionalize 100 nm SiO_2 nanoparticles with an aminosilane group, thus rendering the particles positively charged at neutral to low pH and facilitating the adsorption of the polyanion via electrostatic interactions.^{30,31} The full characterization of the functionalization of SiO_2 to $\text{SiO}_2\text{NH}_3^+$ and of the adsorption of MPS-PPV onto these particles by transmission electron microscopy (TEM), dynamic light scattering (DLS), and UV-vis and fluorescence spectroscopy is described in the Supporting Information section (Figures S1–S4). A 23-fold emission enhancement and a new shoulder at 585 nm were observed in the emission spectrum of MPS-PPV adsorbed on the NPs immediately after mixing with the DOTAP liposomes (Figure 1A, see also normalized emission spectra, Figure S5). Our results are consistent with DOTAP liposomes triggering a reorganization and deaggregation of the polymer adsorbed onto the surface of the NPs,^{21,37} where electrostatic and hydrophobic interactions with DOTAP presumably surpass the electrostatic interaction of the polymer with the aminosilanized surface of the NP.

Adsorption versus Rupture of Liposomes Visualized at the Single-NP Level. To study the interaction dynamics

with DOTAP liposomes and to better understand the mechanistic stages (liposome adsorption, deformation, and rupture, if any),^{10,38,39} we monitored individual polymer-coated nanoparticles using a TIRFM setup adapted with an electron-multiplied charge-coupled device (EM-CCD) camera. Our setup allows for the simultaneous tracking of hundreds of individual NPs in parallel with 100 ms time resolution; in this way, the interaction dynamics can be determined for each NP and liposome independently and the extent to which all NPs and liposomes behave homogeneously can be assessed.³⁹ Dilute solutions of MPS-PPV-coated NPs were injected into preassembled chambers where they adsorbed on top of aminosilanized glass coverslips. The polymer-coated NPs were next excited using a 488 or a 514 nm laser, and the fluorescence intensity of hundreds of individual NPs was monitored over time at an acquisition rate of 10 frames/s. Liposome solutions were flowed through the imaging chamber at a rate of $5 \mu\text{L}/\text{min}$ during image acquisition to record the interaction of incoming liposomes with surface-bound nanoparticles.

Upon flowing a 13 nM solution of DOTAP liposomes (100 nm in diameter), all of the polymer-coated NPs simultaneously showed a stark increase in emission intensity with the arrival of the liposomes (Figure 1B). The intensity enhancement calculated by dividing the intensity recorded at the peak by the intensity recorded immediately before the enhancement for 200 individual NPs was 24-fold (± 11) on average, similar to that in ensemble solution studies (Figure 1A). Under our experimental conditions, nonspecific binding of the positively charged DOTAP liposomes onto the positively charged aminosilanized glass surface was not observed (Figure S6).

We were intrigued by the liposome–NP interaction mechanism accounting for the observed MPS-PPV enhancement. Upon considering that the MPS-PPV-coated NPs have a mean diameter of 110 nm, the average 100-nm-diameter liposomes we initially flowed had enough lipid content each to form a complete (or nearly complete) supported lipid bilayer (SLB)^{10,40,41} on a single NP upon liposome rupture. In this case, the entire surface of the NP would be in contact with the membrane and the emission enhancement is expected to be maximal. In contrast, liposome adsorption and deformation (but no rupture) would render only the fraction of the NP that is in contact with the membrane highly emissive, and the emission enhancement is then expected to be submaximal.

To test whether the liposomes were adsorbing but remaining intact on the surface of the NPs or if they were rupturing to form SLBs, we next measured intensity enhancements under a low concentration of 100-nm-diameter liposomes (0.13 nM, a 100-fold reduction) in order to record single NP–liposome encounters and determine whether the enhancements were submaximal or maximal, respectively. Under these conditions, only 20% of the single-particle fluorescence intensity versus time trajectories showed an enhancement over the 150 s image acquisition time (Figure 2A). The majority of NPs experienced no encounters with liposomes (and thus no emission enhancement), and a subset of particles, ca. 2%, experienced two encounters during the acquisition time, recorded as two distinct intensity jumps of comparable amplitude. The onset of the enhancement was random over time, consistent with the fact that NPs and liposomes have a low encounter probability when liposomes are flowed at this low concentration. The mean enhancement measured for 170 individual NPs was 5.4 ± 2.8 -fold for the 100 nm liposomes, ca. 5-fold smaller than the maximum value recorded under excess liposomes for the same NPs. Given this value, we estimated that 20% of the total area of the NP was in contact with a 100 nm liposome on average, in line with a liposome interacting and plausibly deforming on an NP surface rather than with its rupture to form an SLB^{10,40,41} (see also cryo-TEM studies, *vide infra*). The fact that only 20% of the NP surface area was occupied by the adsorbed liposome also opened the possibility of the adsorption of additional liposomes. Indeed, when the liposome concentration was raised 10-fold to 1.3 nM, the fluorescence intensity versus time trajectories of the NPs showed several discrete enhancement “steps” (Figure 2B), each of roughly the same magnitude as the single steps recorded at the 0.13 nM liposome concentration (Figure 2A). The steps were attributed to the interaction of multiple liposomes on a single NP. As described above, in the presence of the 1.3 nM liposome solution the onset of the fluorescence enhancement for MPS-PPV-coated NPs was simultaneous; that is, every NP began to be enhanced at approximately the same time (Figure 2C), and the mean enhancement was 24-fold. At this concentration, individual liposome–NP encounter events were not well resolved.

We reasoned that larger liposomes may be capable of “engulfing” a larger portion of the NP while still remaining intact, thus leading to larger intensity enhancements. When low concentrations (ca. 0.08 nM) of larger liposomes (up to 400 nm in diameter) were flowed over the NPs, single-step intensity enhancements of up to 23-fold were observed (Figure 2D). These enhancements were suggestive of a liposome population possessing a large enough lipid surface area to fully wrap around the NPs upon deformation, leading to complete polymer deaggregation/reorganization and a maximal fluo-

rescence enhancement. Given the large polydispersity of the liposome sample (Figure 2E), however, many smaller enhancements were also observed and the average enhancement calculated for 170 individual NPs was $10.7(\pm 8)$ -fold. The large distribution in intensity enhancements for the 400 nm sample was correlated with its relatively large polydispersity. By comparison, a narrower enhancement distribution was observed for the 100-nm-diameter liposomes which were also characterized by a smaller polydispersity (Figure 2E,F). Upon flowing a 100-fold-larger concentration of 400 nm liposomes, the fluorescence enhancement was simultaneous in time for all particles, and the mean intensity enhancement was $22(\pm 10)$ -fold (versus $24(\pm 11)$ -fold for 100 nm liposomes under similar conditions). Under high liposome concentrations the distribution of enhancements is furthermore indistinguishable between the 100 and 400 nm liposome populations (Figure S7).

Overall, we observed that the enhanced intensity of the MPS-PPV-coated NPs was positively correlated to the initial intensity of the NPs when the liposomes were flowed in large excess and were not a limiting reagent (Figure 2G). The linear correlation is consistent with a relatively uniform deposition of MPS-PPV on a particle-to-particle basis, where the major difference between the NPs is the size of the underlying SiO₂ NP support. The distribution of initial intensities was observed to be correlated with the distribution of sizes observed by dynamic light scattering measurements (Figure S8). The presence of more adsorbed polymer on a NP with a larger surface area will in turn lead to a larger initial intensity and a larger enhanced intensity, assuming that every NP has an equal ability to interact with the liposomes and attain a maximal enhancement. In line with the above, when the same liposomes were flowed at a 100-fold-lower concentration (Figure 2H) the initial intensity was not correlated to the enhanced intensity. The convergence of the size distribution of NPs (Figure S2) and the size distribution of interacting liposomes (Figure 2E) at 1:1 stoichiometry resulted in the poor correlation observed.

To gain a molecular-level visualization of the interaction of the MPS-PPV-coated NPs and DOTAP liposomes we performed cryo-TEM studies. MPS-PPV-coated NPs were added to excess DOTAP liposomes, and the sample was vitrified within 30 s following mixing. At this stage, many liposomes of varying size were adsorbed onto the MPS-PPV-coated NPs, as revealed by the ring of electron-dense material 4 to 5 nm from the edge of the NPs (Figure 3A,B). The adsorbed liposomes were deformed⁴² to varying degrees to accommodate the curvature of the NP surface. The engulfment of NPs by larger liposomes was observed as we proposed on the basis of our TIRFM studies (arrow 2 in Figure 3A). On some particles, fully formed supported lipid bilayers (SLBs) were observed¹⁰ (arrow 1 in Figure 3A), but whereas the majority of NPs had one or more adsorbed liposomes (arrow 3 in Figure 3B), the presence of a fully formed SLB was rare. Importantly, upon prolonged incubation of liposomes and NPs for 30 min and following the removal of the excess liposomes by centrifugation, cryo-TEM images showed completely formed SLBs on all of the NPs (Figure 3D,F). Given that some SLBs are already observed within 30 s of mixing we believe that SLB formation is the final fate of the system at long time scales, although it remains an open question as to whether mechanical disruption of the liposomes during the centrifugation step may have accelerated this process. More importantly, however, is the fact that it is unlikely that liposome rupture was responsible for the MPS-PPV emission enhancements observed during the TIRFM

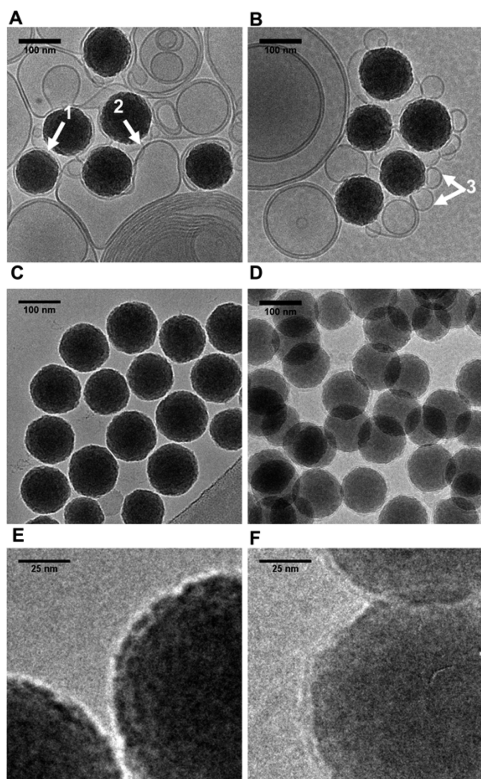


Figure 3. Cryo-TEM micrographs of MPS-PPV-coated SiO_2 NPs with 400 nm DOTAP liposomes. (A, B) A solution containing NPs and liposomes was vitrified within 30 s following mixing of the liposomes and the NPs. Arrow 1 points to a fully formed SLB on an NP, arrow 2 points to a large liposome deformed around the surface of an NP, and arrow 3 points to multiple small liposomes adsorbed on the same NP. (C) MPS-PPV-coated NPs. (D) MPS-PPV-coated NPs that were incubated with DOTAP liposomes prior to the removal of the excess liposomes by centrifugation. (E, F) Close-up views of images in panels C and D, respectively. The concentration of NPs was 1 nM, and the concentration of 400-nm-diameter DOTAP liposomes was 8 nM. The samples were suspended in a 3 mM NaCl aqueous solution.

microscopy experiments given that these enhancements were found to occur on the tens of milliseconds time scale whereas the near absence of completely formed SLBs in TEM images obtained 30 s following mixing suggested that liposome rupture is a slower process in this system. Dye leakage experiments of red emissive fluorophore Cy5 encapsulated inside liposomes in the presence of external quencher FeCl_3 further showed that the majority of liposomes do not rupture within 10 min of mixing with MPS-PPV-coated NPs (Figure S9).

A closer inspection of the cryo-TEM micrographs further revealed the close proximity between the membrane and the polymer-coated NP. Considering a 4- to 5-nm-thick bilayer, one may infer that the thickness of the water layer separating the inner lipid leaflet from the NP^{43,44} is at most 1 nm. Under our resolution it was not possible to distinguish either the inner membrane leaflet or the outer leaflet regardless of whether one observed regions of membrane in contact with NPs or free in vitreous aqueous solution; however, both sections of the membrane (i.e., free in solution or in contact with the NP) were identical, revealing that the interaction with MPS-PPV did not result in membrane thickening. Importantly, the bilayer closely follows the underlying SiO_2 NP topography (Figure 3), indicating that the polyelectrolyte does not significantly shield the membrane from the underlying surface roughness.

Liposome–NP Interaction Dynamics and Ensuing Polymer Deaggregation.

In subsequent experiments we sought to simultaneously visualize the liposomes and the surface-bound polymer-coated NPs in parallel channels in order to unequivocally establish their interaction dynamics upon liposome arrival. Experimentally, we labeled the DOTAP liposomes with red, lipophilic dye DiD in a lipid to DiD molar ratio of 256:1. Both MPS-PPV and DiD were excited with a 514 nm laser. The emission was collected and split into a red (DiD) and a green (MPS-PPV-coated NPs) channel using a 640 nm beamsplitter. NPs were located in the green channel, and the corresponding region was mapped in the red channel to allow us to monitor the appearance of DiD-stained liposomes as the solution flowed in (Figure 4).

The concentration of the 400 nm liposome solution that flowed during imaging was optimized to 0.080 nM liposomes so that the majority of NPs (81%) did not interact with a liposome during the image acquisition time. The intensity–time trajectories for these NPs in the green channel displayed an exponentially decaying intensity arising from the photobleaching of MPS-PPV, and the intensity recorded in the red channel mirrored the green channel due to 25% crosstalk. In the remaining trajectories, the colocalization of a red-emissive liposome with a green-emissive NP was signaled by a rapid increase in the fluorescence intensity monitored in the red channel occurring over a maximum of two 100 ms frames. A total of 17% of the trajectories showed the colocalization of one liposome, and 2% of the trajectories showed the colocalization of a second liposome. Monitoring both channels simultaneously enabled us to unequivocally establish that every encounter between a liposome and an NP was irreversible (i.e., liposomes did not dock and undock) over the time period observed. Furthermore, we recorded no nonproductive liposome–NP encounters (i.e., upon docking, DOTAP liposomes triggered the rapid deaggregation of MPS-PPV in all cases).

The two-color TIRFM experiments additionally showed that the MPS-PPV intensity enhancement recorded was directly proportional to the incoming liposome size (Figure 5A), a result that was consistent with the larger enhancements observed on average when larger liposomes were flowed over polymer-coated NPs in one-color experiments (Figure 2E,F, *vide supra*). Considering a random distribution of DiD molecules in the lipid membrane, the number of dyes present and thus the intensity of any given liposome are directly proportional to the lipid surface area (i.e., larger liposomes are brighter).⁴⁵ The intensity of the incoming liposome in the red channel was positively correlated to the intensity enhancement of MPS-PPV in the green channel (Figure 5A). For the same data set, the change in MPS-PPV fluorescence intensity showed a poor correlation to the initial intensity of the NP (Figure 5B), consistent with the idea that it is primarily the size of the liposome (amount of lipid entering in contact with MPS-PPV, triggering deaggregation) and not the total amount of MPS-PPV present in an NP that determines the size of the enhancement.

The MPS-PPV enhancement period, defined as the number of frames that elapsed from the onset of MPS-PPV emission enhancement until its peak value is reached, was also investigated with results from the one-color TIRFM experiments as convolution between FRET and DiD photobleaching hampers this study with the two-color data. The fluorescence versus time trajectories of MPS-PPV-coated NPs interacting with individual 100 and 400 nm liposomes (Figure 2A,D,

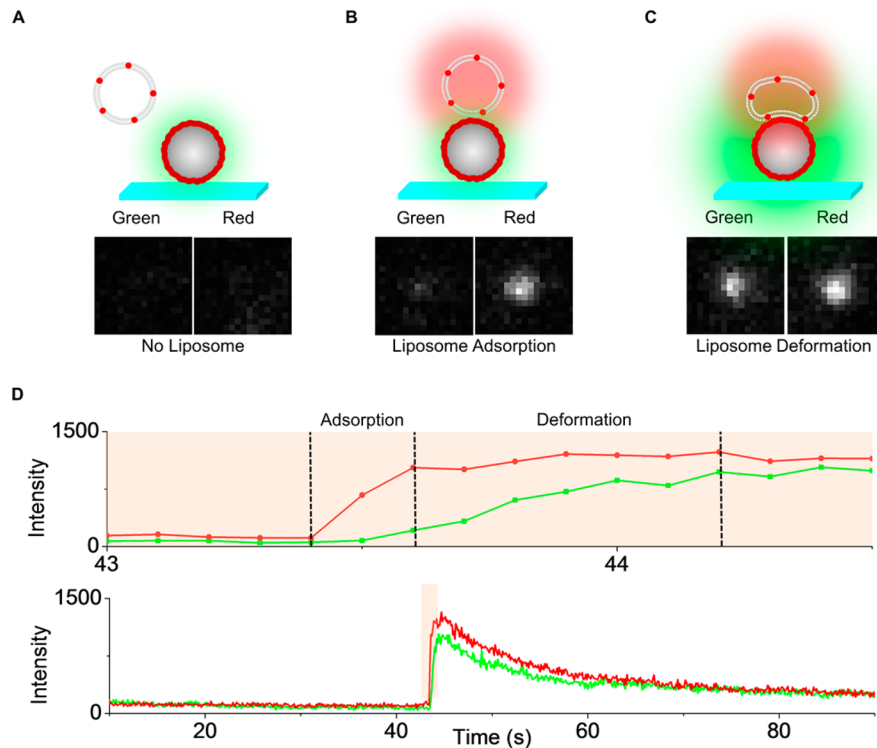


Figure 4. Simultaneous visualization of the encounter of a single DOTAP liposome and an MPS-PPV-coated NP. Surface-immobilized MPS-PPV-coated NPs were excited with the $580\ \mu\text{W}$ output of a 514 nm laser, and TIRFM images were obtained at a time resolution of 10 frames/s. DOTAP liposomes (400 nm) labeled with DiD in a 256:1 lipid/dye ratio at a concentration of 0.08 nM in 3 mM NaCl were flowed at a rate of $5\ \mu\text{L}/\text{min}$ during imaging. (A) Dimly emissive MPS-PPV-coated NPs are initially visible in the green channel. (B) The colocalization of a DiD-labeled liposome with a NP was signaled by the appearance of a fluorescence signal in the red channel over a period of one or two frames. (C) The colocalization of the liposome triggered the onset of the MPS-PPV fluorescence enhancement. (D) Representative fluorescence intensity versus time trajectory for an NP interacting with a DOTAP liposome in a two-channel experiment. The full trajectory is shown at the bottom. Highlighted is the portion where the incoming liposome interacts with the NP, shown in greater detail at the top.

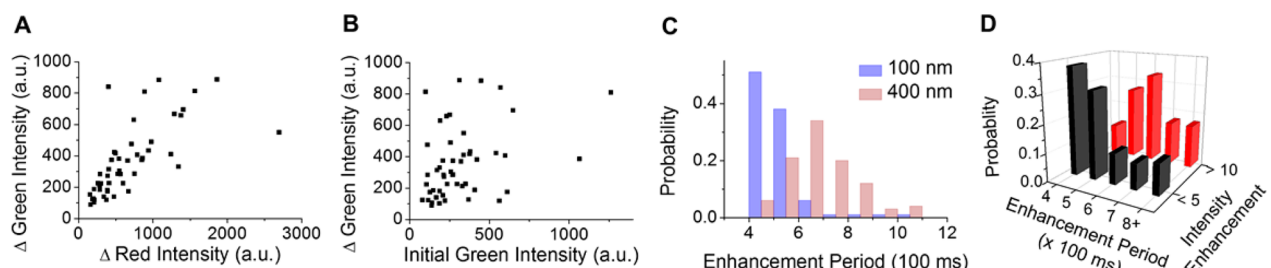


Figure 5. Correlation between the emission enhancement magnitude and the enhancement period for an MPS-PPV-coated NP versus liposome size. (A) Correlation plot of the enhanced MPS-PPV intensity in the green emission channel versus the intensity of the dye-labeled liposome in the red emission channel. (B) Correlation plot of the enhanced MPS-PPV emission intensity versus the initial MPS-PPV emission intensity. (C) Distribution of enhancement periods for both 100 nm and 400 nm liposomes. (D) Distribution of NPs with enhancements of less than 5-fold and enhancements greater than 10-fold sorted by their enhancement periods plotted for NPs interacting with 100- and 400-nm-diameter liposomes. Graphs A and B are plotted using data from two-color TIRFM experiments utilizing 400 nm DOTAP liposomes labeled with DiD in a 256:1 lipid/dye ratio. Surface-bound MPS-PPV-coated NPs were excited with a 514 nm laser ($500\ \mu\text{W}$), and their emission intensity was monitored while flowing liposomes at a concentration of 0.08 nM in 3 mM NaCl. Graphs C and D are plotted using data from one-color TIRFM experiments utilizing $100\text{ and }400\text{ nm}$ DOTAP liposomes in 3 mM NaCl flowed at concentrations of 0.13 and 0.08 nM , respectively. Here, the excitation source was a 488 nm laser ($220\ \mu\text{W}$). All liposome solutions were flowed at a rate of $5\ \mu\text{L}/\text{min}$, and images were acquired with a time resolution of 10 fps.

respectively) were analyzed, and the distribution of enhancement periods is shown in Figure 5C. The mean enhancement period was $430(\pm 70)\text{ ms}$ for the 100 nm liposome sample and slightly longer, $630(\pm 110)\text{ ms}$, for the 400 nm liposome sample. The fluorescence enhancement for each NP was also determined. The NPs were sorted into groups based on the size of their enhancement, and the probability of having a given enhancement period within each group was determined (Figure

5D). Liposomes triggering smaller enhancements (less than 5-fold) were more likely to have shorter enhancement periods whereas liposomes triggering larger enhancements (greater than 10-fold) were more likely to have longer enhancement periods. Given the positive correlation observed between liposome size and enhancement size in the experiments with dye-labeled liposomes, we may conclude that smaller liposomes are more likely to induce rapid deaggregation of MPS-PPV than

larger liposomes. The exact nature of the microscopic rearrangements taking place between the polymer and the liposome is unclear. It is plausible that liposome deformation is the rate-limiting step and that larger liposomes, which have a higher possibility to deform, take longer to explore the surface of the NP than smaller liposomes whose interaction area is more limited.

CONCLUSIONS

We provide a methodology to measure the dynamics of membrane deformation for a membrane in contact with polyelectrolyte scaffolding. Utilizing single-particle fluorescence and exploiting the spectroscopic properties of conjugated polyelectrolytes, which are dimly emissive when aggregated yet highly emissive upon conformational reorganization in the presence of surfactants, including lipids, we are able to record real-time liposome docking and subsequent deformation on the surface of SiO_2 nanoparticles coated with a conjugated polyelectrolyte. Conformational changes in the conjugated polyelectrolyte as the membrane deforms along the surface curvature of the nanoparticle results in fluorescence intensity enhancements. These enhancements are proportional to the surface coverage by the lipid milieu, providing a means to read to which extent the membrane deforms and how rapidly it is doing so. Larger liposomes, which have a higher possibility to deform, take longer to explore the surface of the NP than smaller liposomes whose interaction area is more limited. Cryo-TEM studies provide a molecular-level (structural) visualization of the resulting products. Multiple small liposomes are observed interacting with single NPs, and larger liposomes readily engulf a single conjugated polyelectrolyte-coated NP. The adsorbed liposomes underwent varying extents of deformation such that the membrane closely followed the topology of the underlying SiO_2 support. Liposome rupture at longer times ultimately leads to the formation of supported lipid bilayers.

We believe that the development of our approach will enable the interrogation of the dynamics at play as model membranes and cell membranes adjust their phase and topology in the presence of charged scaffoldings. Wisely chosen conjugated polyelectrolyte composites may enable the role of charge and hydrophobic interactions between the membrane and the scaffolding to be reported spectroscopically. Different lipids and lipid mixtures may be monitored, yielding additional information on the role of chemical composition. Physical parameters such as the curvature of the liposomes and the NPs and their role in membrane dynamics could be easily followed.

ASSOCIATED CONTENT

Supporting Information

Characterization of MPS-PPV-coated NPs by TEM, DLS, and UV-vis and fluorescence spectroscopy; control experiments to determine the nonspecific adsorption of DOTAP liposomes on aminosilanized glass coverslips; histogram of MPS-PPV-coated NP emission enhancement while conducting TIRFM experiments with high concentrations of 100 and 400 nm DOTAP liposomes; dye leakage experiments of encapsulated fluorophores to determine the extent of DOTAP liposome rupture. The Supporting Information is available free of charge on the ACS Publications website at DOI: 10.1021/acs.langmuir.Sb00979.

AUTHOR INFORMATION

Corresponding Author

*E-mail: gonzalo.cosa@mcgill.ca.

Author Contributions

C.F.C. and H.-W.L. acquired the data. All authors contributed ideas and discussed the results. C.F.C. and G.C. wrote the article, and G.C. designed and coordinated the study.

Notes

The authors declare no competing financial interest.

ACKNOWLEDGMENTS

G.C. is thankful to the National Science and Engineering Research Council of Canada (NSERC) and the Canada Foundation for Innovation (CFI). We are thankful to McGill CIHR drug development training program DDTP and GRASP for postgraduate scholarships to H.-W.L. We also thank NSERC for a graduate scholarship to C.F.C.

REFERENCES

- (1) McMahon, H. T.; Gallop, J. L. Membrane curvature and mechanisms of dynamic cell membrane remodelling. *Nature* **2005**, *438*, 590–596.
- (2) Baumgart, T.; Capraro, B. R.; Zhu, C.; Das, S. L. Thermodynamics and Mechanics of Membrane Curvature Generation and Sensing by Proteins and Lipids. *Annu. Rev. Phys. Chem.* **2011**, *62*, 483–506.
- (3) Zimmerberg, J.; Kozlov, M. M. How proteins produce cellular membrane curvature. *Nat. Rev. Mol. Cell Biol.* **2006**, *7*, 9–19.
- (4) Brown, M. F. Curvature Forces in Membrane Lipid–Protein Interactions. *Biochemistry* **2012**, *51*, 9782–9795.
- (5) Stachowiak, J. C.; Brodsky, F. M.; Miller, E. A. A cost-benefit analysis of the physical mechanisms of membrane curvature. *Nat. Cell Biol.* **2013**, *15*, 1019–1027.
- (6) Koltover, I.; Salditt, T.; Rädler, J. O.; Safinya, C. R. An Inverted Hexagonal Phase of Cationic Liposome-DNA Complexes Related to DNA Release and Delivery. *Science* **1998**, *281*, 78–81.
- (7) Caracciolo, G.; Amenitsch, H. Cationic liposome/DNA complexes: from structure to interactions with cellular membranes. *Eur. Biophys. J.* **2012**, *41*, 815–829.
- (8) Tanaka, M.; Sackmann, E. Polymer-supported membranes as models of the cell surface. *Nature* **2005**, *437*, 656–663.
- (9) Berti, D.; Caminati, G.; Baglioni, P. Functional liposomes and supported lipid bilayers: towards the complexity of biological archetypes. *Phys. Chem. Chem. Phys.* **2011**, *13*, 8769–8782.
- (10) Mornet, S.; Lambert, O.; Duguet, E.; Brisson, A. The Formation of Supported Lipid Bilayers on Silica Nanoparticles Revealed by Cryoelectron Microscopy. *Nano Lett.* **2004**, *5*, 281–285.
- (11) Golan, S.; Salmon, Y. Nanostructure of Complexes Between Cationic Lipids and an Oppositely Charged Polyelectrolyte. *Langmuir* **2012**, *28*, 1668–1672.
- (12) Bershteyn, A.; Chaparro, J.; Yau, R.; Kim, M.; Reinherz, E.; Ferreira-Moita, L.; Irvine, D. J. Polymer-supported lipid shells, onions, and flowers. *Soft Matter* **2008**, *4*, 1787–1791.
- (13) Frost, A.; Perera, R.; Roux, A.; Spasov, K.; Destaing, O.; Egelman, E. H.; De Camilli, P.; Unger, V. M. Structural Basis of Membrane Invagination by F-BAR Domains. *Cell* **2008**, *132*, 807–817.
- (14) Bolinger, J. C.; Traub, M. C.; Brazard, J.; Adachi, T.; Barbara, P. F.; Vanden Bout, D. A. Conformation and Energy Transfer in Single Conjugated Polymers. *Acc. Chem. Res.* **2012**, *45*, 1992–2001.
- (15) Schwartz, B. J. Conjugated Polymers as Molecular Materials: How Chain Conformation and Film Morphology Influence Energy Transfer and Interchain Interactions. *Annu. Rev. Phys. Chem.* **2003**, *54*, 141–172.

- (16) Kobayashi, H.; Onda, S.; Furumaki, S.; Habuchi, S.; Vacha, M. A single-molecule approach to conformation and photophysics of conjugated polymers. *Chem. Phys. Lett.* **2012**, *528*, 1–6.
- (17) Huser, T.; Yan, M.; Rothberg, L. J. Single chain spectroscopy of conformational dependence of conjugated polymer photophysics. *Proc. Natl. Acad. Sci. U.S.A.* **2000**, *97*, 11187–11191.
- (18) Ebihara, Y.; Vacha, M. Relating Conformation and Photophysics in Single MEH-PPV Chains. *J. Phys. Chem. B* **2008**, *112*, 12575–12578.
- (19) Bout, D. A. V.; Yip, W.-T.; Hu, D.; Fu, D.-K.; Swager, T. M.; Barbara, P. F. Discrete Intensity Jumps and Intramolecular Electronic Energy Transfer in the Spectroscopy of Single Conjugated Polymer Molecules. *Science* **1997**, *277*, 1074–1077.
- (20) Heeley, M. E. H.; Gallaher, J. K.; Nguyen, T. L.; Woo, H. Y.; Hodgkiss, J. M. Surfactant controlled aggregation of conjugated polyelectrolytes. *Chem. Commun. (Cambridge, U. K.)* **2013**, *49*, 4235–4237.
- (21) Chen, L.; Xu, S.; McBranch, D.; Whitten, D. Tuning the Properties of Conjugated Polyelectrolytes through Surfactant Complexation. *J. Am. Chem. Soc.* **2000**, *122*, 9302–9303.
- (22) Costa, T.; Garner, L. E.; Knapila, M.; Thomas, A. W.; Rogers, S. E.; Bazan, G. C.; Burrows, H. D. Aggregation Properties of p-Phenylene Vinylene Based Conjugated Oligoelectrolytes with Surfactants. *Langmuir* **2013**, *29*, 10047–10058.
- (23) Dou, W.; Wang, C.; Wang, G.; Ma, Q.; Su, X. Enhance Effect of Surfactants on the Photoluminescence and Photostability of Water-Soluble Poly(phenylene ethynylene). *J. Phys. Chem. B* **2008**, *112*, 12681–12685.
- (24) Ngo, A. T.; Cosa, G. Assembly of Zwitterionic Phospholipid/Conjugated Polyelectrolyte Complexes: Structure and Photophysical Properties. *Langmuir* **2009**, *26*, 6746–6754.
- (25) Karam, P.; Hariri, A. A.; Calver, C. F.; Zhao, X.; Schanze, K. S.; Cosa, G. Interaction of Anionic Phenylene Ethynylene Polymers with Lipids: From Membrane Embedding to Liposome Fusion. *Langmuir* **2014**, *30*, 10704–10711.
- (26) Karam, P.; Ngo, A. T.; Rouiller, I.; Cosa, G. Unraveling electronic energy transfer in single conjugated polyelectrolytes encapsulated in lipid vesicles. *Proc. Natl. Acad. Sci. U.S.A.* **2010**, *107*, 17480–17485.
- (27) Zeineldin, R.; Piyasena, M. E.; Sklar, L. A.; Whitten, D.; Lopez, G. P. Detection of Membrane Biointeractions Based on Fluorescence Superquenching. *Langmuir* **2008**, *24*, 4125–4131.
- (28) Wang, Y.; Schanze, K. S.; Chi, E. Y.; Whitten, D. G. When Worlds Collide: Interactions at the Interface between Biological Systems and Synthetic Cationic Conjugated Polyelectrolytes and Oligomers. *Langmuir* **2013**, *29*, 10635–10647.
- (29) Garner, L. E.; Park, J.; Dyar, S. M.; Chworus, A.; Sumner, J. J.; Bazan, G. C. Modification of the Optoelectronic Properties of Membranes via Insertion of Amphiphilic Phenylenevinylene Oligoelectrolytes. *J. Am. Chem. Soc.* **2010**, *132*, 10042–10052.
- (30) Ngo, A. T.; Lau, K. L.; Quesnel, J. S.; Aboukhailil, R.; Cosa, G. Deposition of anionic conjugated poly(phenylenevinylene) onto silica nanoparticles via electrostatic interactions — Assembly and single-particle spectroscopy. *Can. J. Chem.* **2011**, *89*, 385–394.
- (31) Liu, H.-W.; Ngo, A. T.; Cosa, G. Enhancing the Emissive Properties of Poly(p-phenylenevinylene)-Conjugated Polyelectrolyte-Coated SiO₂ Nanoparticles. *J. Am. Chem. Soc.* **2011**, *134*, 1648–1652.
- (32) Jiang, H.; Taranekar, P.; Reynolds, J. R.; Schanze, K. S. Conjugated Polyelectrolytes: Synthesis, Photophysics, and Applications. *Angew. Chem., Int. Ed.* **2009**, *48*, 4300–4316.
- (33) Liu, B.; Bazan, G. C. *Conjugated Polyelectrolytes: Fundamentals and Applications*; Wiley-VCH Verlag GmbH & Co. KGaA: Weinheim, Germany, 2012.
- (34) Ngo, A. T.; Karam, P.; Cosa, G. Conjugated polyelectrolyte-lipid interactions: Opportunities in biosensing. *Pure Appl. Chem.* **2011**, *83*, 43–55.
- (35) Wang, Y.; Jones, E. M.; Tang, Y.; Ji, E.; Lopez, G. P.; Chi, E. Y.; Schanze, K. S.; Whitten, D. G. Effect of Polymer Chain Length on Membrane Perturbation Activity of Cationic Phenylene Ethynylene Oligomers and Polymers. *Langmuir* **2011**, *27*, 10770–10775.
- (36) Roy, R.; Hohng, S.; Ha, T. A practical guide to single-molecule FRET. *Nat. Methods* **2008**, *5*, 507–516.
- (37) Dalvi-Malhotra, J.; Chen, L. Enhanced Conjugated Polymer Fluorescence Quenching by Dipyradimium-Based Quenchers in the Presence of Surfactant. *J. Phys. Chem. B* **2005**, *109*, 3873–3878.
- (38) Troutier, A.-L.; Ladavière, C. An overview of lipid membrane supported by colloidal particles. *Adv. Colloid Interface Sci.* **2007**, *133*, 1–21.
- (39) Johnson, J. M.; Ha, T.; Chu, S.; Boxer, S. G. Early Steps of Supported Bilayer Formation Probed by Single Vesicle Fluorescence Assays. *Biophys. J.* **2002**, *83*, 3371–3379.
- (40) Hamai, C.; Cremer, P. S.; Musser, S. M. Single Giant Vesicle Rupture Events Reveal Multiple Mechanisms of Glass-Supported Bilayer Formation. *Biophys. J.* **2007**, *92*, 1988–1999.
- (41) Takáts-Nyeste, A.; Derényi, I. Development of Hat-Shaped Liposomes on Solid Supports. *Langmuir* **2014**, *30*, 15261–15265.
- (42) Reviakine, I.; Gallego, M.; Johannsmann, D.; Tellechea, E. Adsorbed liposome deformation studied with quartz crystal microbalance. *J. Chem. Phys.* **2012**, *136*, -.
- (43) Raedler, J.; Streij, H.; Sackmann, E. Phenomenology and Kinetics of Lipid Bilayer Spreading on Hydrophilic Surfaces. *Langmuir* **1995**, *11*, 4539–4548.
- (44) Bayerl, T. M.; Bloom, M. Physical properties of single phospholipid bilayers adsorbed to micro glass beads. A new vesicular model system studied by 2H-nuclear magnetic resonance. *Biophys. J.* **1990**, *58*, 357–362.
- (45) Larsen, J.; Hatzakis, N. S.; Stamou, D. Observation of Inhomogeneity in the Lipid Composition of Individual Nanoscale Liposomes. *J. Am. Chem. Soc.* **2011**, *133*, 10685–10687.